Available online at www.sciencedirect.com

ScienceDirect

Procedia CIRP 114 (2022) 73–78

www.elsevier.com/locate/procedia

17th CIRP Conference on Computer Aided Tolerancing

Effect of filters on segmentation-free geometric verification by X-ray CT

Stefano Petrò[a,*], Giovanni Moroni[a]

[a]*Department of Mechanical Engineering, Politecnico di Milano, Via Giuseppe La Masa, 20156 Milano, Italy*

Abstract

A method has been proposed to verify geometric tolerances by X-ray computed tomography (XCT) without the need for image segmentation. The method is based on the direct comparison of a part XCT image to a volumetric representation of its geometric tolerance. In previous works the method was directly applied to raw images. However, filters are commonly applied to XCT images. Usually, they mitigate noise or enhance details. In this work, we study if the segmentation-free verification benefits from the application of filters to XCT images. Standard filters are considered, e.g. Gaussian and non-local means.

Keywords: X-ray computed tomography; geometric inspection; segmentation; volumetric representation; filtering.

1. Introduction

Additive manufacturing (AM) sets new rules. New rules for design, which can now take advantage of an (almost) complete freedom of the possible geometries [28, 29]. New rules for manufacturing, were the new systems requires different policies for management and logistics, not to mention different operator's qualifications [3, 25]. And also metrology has new rules, as most conventional measuring systems are limited when facing the complex and undercut geometries typical of AM [15, 24]. Such revolution requires the whole process of designing, manufacturing, and inspecting to be rethought.

Concerning the need for an AM-focused renewal of practices, in previous works the authors proposed to move from the conventional surface representation of parts to volumetric representations [18, 17, 19, 20, 21]. Volumetric representations guarantee an absolute freedom of design. In practice, in a volumetric representation part characteristics are defined point-by-point in the definition volume - a 3D image of the part. Design freedom is not limited by the need for regular surfaces or homogeneous characteristics. This is also coherent with the use of topological optimization, which most often works volumetrically [22]. In addition, volumetric representations can be "enriched" to convey information not only on the part geometry, but also on material characteristics, surface properties, local tolerances, etc [26, 18]. For what concerns manufacturing, is worth noting that the conventional .stl slicing process and filling pattern definition actually converts the surface representation into a volumetric representation [2]. Solutions bypassing the need of a surface representation of parts are commercially available [31].

Volumetric representation of geometric tolerances is possible. In principle, it suffices to define of a "minimum material continuum" (the portion of volume that *must* be filled by material) and a "maximum material continuum" (the portion of volume that *can* be filled by material) to specify the part geometry permissible variation [18, 21]. The volume belonging to the maximum material continuum but excluded from the minimum material continuum is the transition (tolerance) zone, which can be either filled with material or not. It is worth noting such representation is flexible, allowing e.g. the definition of non-constant tolerance zones.

This volumetric representation of tolerance zones is also coherent with a geometric verification by X-ray computed tomography (XCT) [14, 7, 5]. XCT, thanks to its flexibility, is the most suitable imaging method for AM part verification [15]. The authors have already illustrated a method for the verification AM part geometry which, differing from the conventional segmentation-based approach, does not require segmentation [17]. Therefore, the method is named "segmentation-free ge-

* Corresponding author. Tel.: +39 02 2399 8530.
E-mail address: stefano.petro@polimi.it (Stefano Petrò).

10.1016/j.procir.2022.10.011

ometric inspection", and is a novel method for the verification of geometrical deviations, particularly effective when AM parts are involved. The main drawback of the original method was the lack of a verification errors management. This is usually obtained in conventional geometric metrology by uncertainty evaluation and guard-bands definition [12, 13]. As the method does not include an actual measurement result, this approach is unfeasible. Recently, the method has been amended, allowing the definition consumer's and producer's risks [21]. This bypasses the need for an estimate of the uncertainty to assess the measurement reliability.

In previous works, segmentation-free geometric inspection has been applied to raw data. This is in contrast with common practices in XCT. Most XCT images are affected by a significant noise. Therefore, it is common to apply them denoising filters before any analysis is performed to mitigate the noise impact. In this work, we analyze how the application of denoising filters affects the result of segmentation-free geometric inspection. For sake of completeness, in §2 segmentation-free geometric inspection is briefly illustrated. §3 introduces the denoising filters considered for comparison. To complete the discussion, in §4 segmentation-free geometric inspection is applied to the same datasets used in a previous work [21] after denoising filters have been applied and the results are described. Finally, §5 draws conclusions on the obtained results.

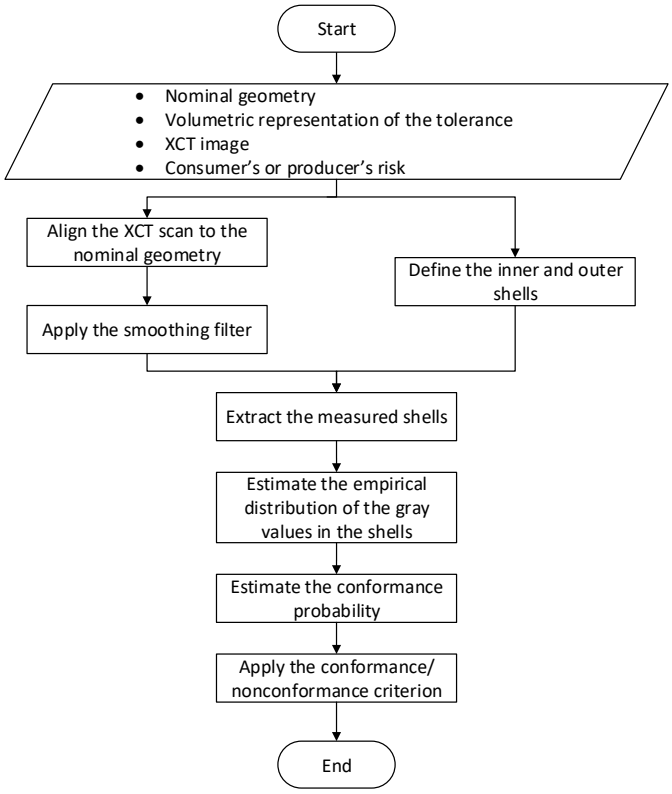

Fig. 1. Flux diagram of the segmentation-free geometric inspection.

2. Segmentation-free geometric inspection

Segmentation-free geometric inspection has been deeply described in previous works, particularly in [21]. For sake of completeness, it is summarized here as well and depicted in Fig. 1.

The data required for the method include:

- the nominal geometry, expressed in a binary 3D image;
- the volumetric representation of the geometric tolerance, expressed in a 3D image;
- the XCT image;
- either the consumer's (conformance test) or the producer's (nonconformance test) risk.

First, the XCT image must be aligned to the nominal geometry. Considering the two are heterogeneous volumetric representations of the same object, it is suggested they are aligned by maximization of the mutual information [23]. In principle this step is unnecessary when the images are externally aligned, e.g. when they are aligned based on some datum features. Once alignment has been obtained, the smoothing filter is applied to the XCT image.

In parallel, the relevant portion of the volume shall be identified. It may be expected that, if the part deviates geometrically or dimensionally, the first portion of the volume affected is the one immediately inside or outside the tolerance zone. Therefore, only these "inner" and "outer" shells are considered in the method. This both reduces the computational burden and increases robustness in presence of porosity and artifacts. Once the shells have been defined and the filter applied, the portion of the XCT image corresponding to the shells is extracted. this is the data required to state whether the part conforms or not.

Now, the idea on which segmentation-free geometric inspection is based is that the only information in the nominal representation of the shells is their "complete separation". If this same information is also in the measured shells, then the real shells are expected to be separated as well and the part is conforming. This can be verified by calculating the mutual information shared by the measured and nominal shells, and comparing it to the entropy of the nominal shells [6]: if the values are equal, then the "complete separation" information is in the measured shells. Unfortunately, due to the presence of measurement errors the obtained statement is not necessarily correct. Its reliability must be established.

To overcome this issue, in a previous work [21] a method to estimate the conformance probability (the probability the part is actually conforming, given the measurement result) was developed. It requires the empirical distribution of the gray values within the measured inner and outer shells to be estimated. Based on this, it is possible to simulate the measurement of the shells and, performing a number of simulations, estimate the conformance probability p'_c. Finally, a conformance/nonconformance criterion is applied to state whether the part conforms or not. The criterion, as suggested in standards [12, 13], distinguishes the two cases in which the verification is performed by either the producer or consumer. In general, the idea is that, when the conformance probability is high, the part is conforming, and when it is low the part is non conforming.

The criterion compares p'_c to either the customer's or producer's risk and decides whether the part conforms or not.

3. Denoising filters

All (2D and 3D) images are affected by noise. Noise is due to several sources, including the corpuscular nature of light, the presence of electrical noise in detectors, the atmospheric perturbation between the object and the detector. Therefore, the resulting observed signal $v(i)$ at pixel/voxel i can be expressed as:

$$v(i) = u(i) + n(i) \tag{1}$$

where $u(i)$ is the theoretical signal in absence of noise, and $n(i)$ is the noise contribution [4]. Denoising filters try to identify the $n(i)$ part of the observed signal and remove it to increase the signal-to-noise ratio of the image. Unfortunately, denoising filters are unable to distinguish noise from small details, making filtered images blurred or even distorted.

Many denoising filters have been proposed for 2D images [4], and several can be applied to XCT 3D images as well [11, 9, 27].

VGStudio MAX 3.4 [30], a well-known 3D image analysis software, has been used to filter the images in this work. The considered filters include:

- Gaussian filter;
- box filter;
- median filter;
- adaptive Gaussian filter;
- non-local means filter.

3.1. Gaussian and box filters

Gaussian [11] and box [16] filters are similar. They both substitute the gray value at voxel i with a weighted average of, in principle, all the other voxels. As this operation is mathematically a convolution, this type of filter is also known as "convolution filter". The possibility of taking advantage of the fast Fourier transform [10] to compute convolution makes this kind of filter very computationally efficient.

The box filter applies a simple local arithmetic average of the voxels in a "neighborhood" of voxel i, that is, a "box" of specified size n centered on voxel i. Higher values of n lead to a higher degree of smoothing, but also to a loss of details. Although the box filter is probably the simplest filter, it is known to lead to poor (highly blurred) results.

In the case of the Gaussian filter, the weight of the average (Gaussian kernel) is specified by

$$G_\sigma(x,y,z) = \frac{1}{\left(\sqrt{2\pi}\sigma\right)^3} e^{-\frac{x^2+y^2+z^2}{2\sigma^2}} \tag{2}$$

where x, y, z is the Cartesian position of the voxel to average with respect to the voxel being filtered, and σ is a specified parameter. Higher values of σ lead to a higher degree of smoothing, but also to a loss of details. The structure of the weighting function guarantees that higher weight is given to the voxels closer to the voxel being filtered. Even if this ensures the Gaussian filter preserves edges in the image better than the box filter, it is not considered a good solution if preserving edges is important.

3.2. Median filter

The median filter is not a convolution filter. However, it is similar to the box filter: it is simply a box filter in which the average is substituted by the median. The median filter is particularly effective at removing outlier values. In addition, the median filter is considered effective at preserving edges, even if this has been questioned [1].

3.3. Adaptive Gaussian filter

As indicated in §3.1, the Gaussian filter tends make edges less definite due to blurring effect. To overcome this defect, the adaptive Gaussian filter [8] has been introduced. The idea is to adaptively change the value of σ in the Gaussian kernel of (2). In particular, the value of σ is expected to be inversely proportional to the local standard deviation of the image. As the high values of the local standard deviation denote the presence of an edge, reducing the kernel σ at these locations locally reduces the blurring effect of the Gaussian filter. Several schemes have been proposed in literature for the reduction of σ. It is unknown what scheme has been selected for VGStudio MAX 3.4.

3.4. Non-local means filter

The non-local means filter [4] was introduced to provide a filter effectively preserving the edges of the image. To do so, the algorithm substitutes the voxel with a weighted average of all other voxels like a convolution filter. However, instead of basing the weight of the average on the distance from the considered voxel, the weight is based on a "similarity measure" of a neighborhood of the considered voxel with the neighborhood of the voxel being averaged (hence the name "non-local means"). In practice, the non-local means filter is a Gaussian filter in which the distance from the voxel being filtered $\sqrt{x^2+y^2+z^2}$ is substituted by the similarity measure $S_{i,j}$ (a normalizing factor differing from $\left(\sqrt{2\pi}\sigma\right)^3$ is needed). The commonly adopted similarity measure between voxel i and voxel j is:

$$S_{i,j} = \left\| v(\mathcal{N}_i) - v\left(\mathcal{N}_j\right) \right\| \tag{3}$$

where $v(\mathcal{N}_i)$ is the set of the gray values in the neighborhood of voxel i. The non-local means filter is considered very effective at preserving the edges of the image. Its main drawback is

Fig. 2. The puppet used in the experiment.

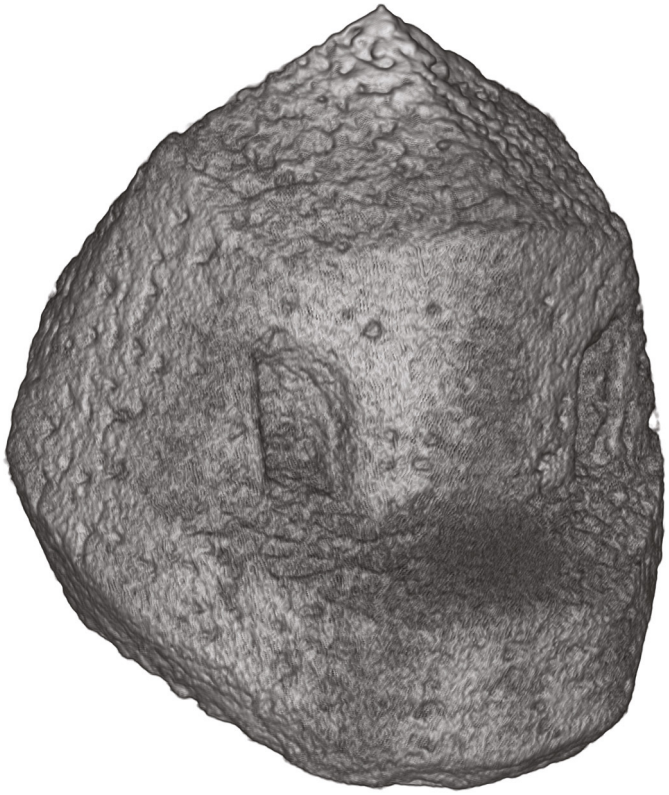

Fig. 3. XCT image of the puppet head.

a computational burden significantly higher than the computational burden of the other filters.

4. Experimental results

The proposed filters have been applied to a series of five XCT images of a metallic puppet shown in Fig. 2. The puppet has been manufactured by selective laser melting of stainless steel. The total height is about 20 mm. The head, in particular, has been imaged 5 times by XCT (Fig. 3). The following scan parameters where adopted:

- voltage: 140 kV;
- current: 47 mA;
- acquisition rate: 13.24 fps;
- number of projections: 600;
- filter: 2.5 mm stainless steel;
- voxel size: 17.67 μm;
- image size: 508(x)x491(y)x439(z) voxels;

The 3D images were aligned to the nominal geometry. Then, the proposed filters were applied using VGStudio MAX 3.4. The selected parameters were as follows:

- Gaussian filter
  - Filter size: 5 voxels
- Box filter
  - Filter size: 5 voxels
- Median filter
  - Filter size: 5 voxels
- Adaptive gaussian filter
  - Smoothing: 0.8
  - Edge threshold: 0.1
- Non-local means filter
  - Smoothing factor: 3

Fig. 4 shows an example of the application of the various filters to a detail of the XCT image.

The application of segmentation-free verification has been deeply described in previous works [20, 21], so it is not discussed here.

The results of the application of segmentation-free verification are summarized in Fig. 5, which shows the estimated probability of conformance p'_c as the amplitude of the transition interval varies, considering the different filters. p'_c is directly proportional to the amplitude of the transition zone, as expected: if the part differs from the nominal geometry, it is more probable it is stated conforming when the tolerance is large. It is apparent that, at some point in the curve, with ranges differing for different filters, p'_c shifts from 0 to 1. Out of the "shifting" range it is then safe to state whether the part is conforming or non conforming. The shifting range instead represents a sort of "uncertainty" range of the method. If the shift is sharper then the range

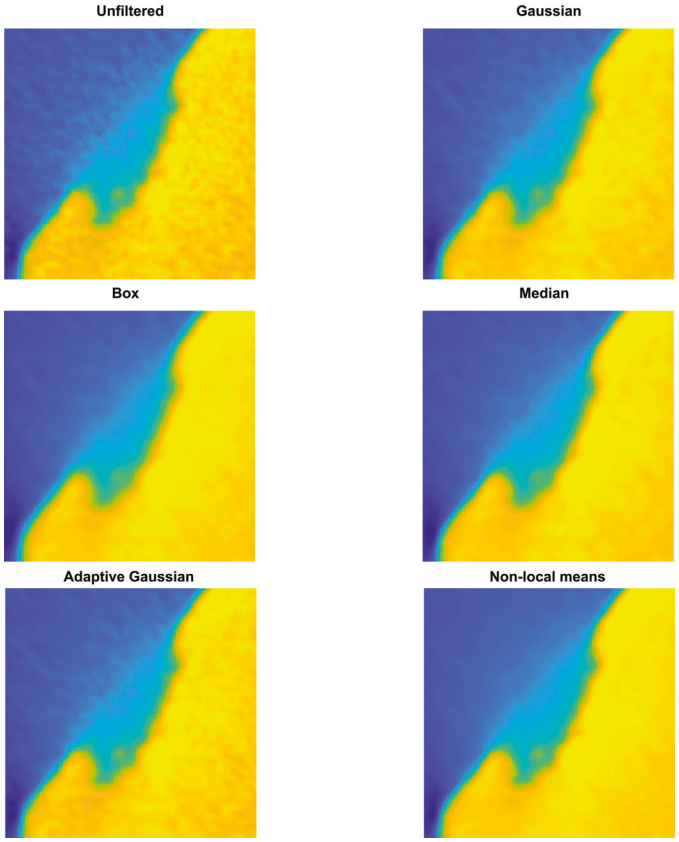

Fig. 4. Example of application of the filters.

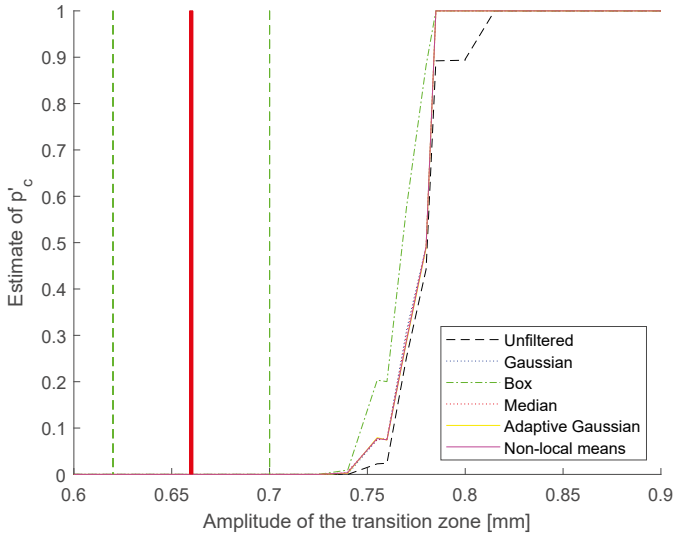

Fig. 5. 95% interval plot of p'_c as the transition interval amplitude varies, for the various filters. The vertical red line indicates the estimated global profile deviation, and the green lines indicate the related coverage interval with a coverage factor equal to 2.

is smaller, which is preferable (smaller uncertainty range). Fig. 5 shows that all curves related to filtered images outperform the unfiltered curve. In particular, the box filter curve seems to outperform all cases. In addition, all "filtered curves" go to the value of 1 before the "unfiltered curve".

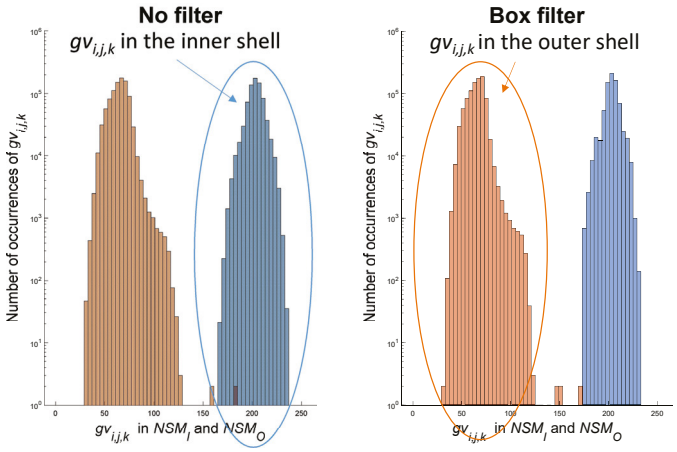

Fig. 6. Histograms of the gray values $gv_{i,j,k}$ in the inner (NSM_i) and outer (NSM_o) measured shells for the fifth measurement replica. Either no filter or box filter was applied to the image.

This can be explained considering Fig. 6, which compares the histograms of the gray values inside the inner and outer shells, for an unfiltered and (box) filtered image. The transition zone in 0.77 mm wide. A few outlying values are clearly visible in both histograms. In the unfiltered histogram, these values, coming from the outer shell, are close and even in the same range of the values of the inner shell. This leads to $p'_c = 0.12$: the part, due to a single value, is stated defective. The application of the filter instead "moves" these values closer to the values of the outer shell: the new estimated value of p'_c is 1, and the part is considered good. This justifies the fact that the filtered curve goes to 1 before the unfiltered curve. It is also apparent that the gray value distribution is characterized by a smaller dispersion in the case of the filtered image than in the unfiltered one. This justifies the sharper switch from 0 to 1: the lower variance makes an overlap of the two histograms of the inner and outer shells less likely.

Finally, even if filters move the transition from 0 to 1 to lower values of the tolerance, the reference value from conventional segmentation and fitting (0.66 mm) is still quite far. Still segmentation-free verification is conservative.

5. Conclusions

Filters are usually applied to XCT images to reduce the effects of noise and artifacts. From the point of view of the information content this reduces the entropy of the signal (sharpening the statistical distributions), and in the end makes easier the "complete separation" of gray values, the core of the segmentation-free verification.

In this work it has been shown that the application of filters tends to reduce the amplitude of the transition zone required to state a part is not defective. It also reduces the uncertainty: by mitigating the effect of outlying gray values and sharpening statistical distributions it is easier to verify whether complete separation holds or not. In the end, it is preferable filters are applied in segmentation-free geometric verification.

The optimal degree of filtering has still to be studied. Using smoother yet edge-preserving filters could lower the estimate of the geometric error, making it closer tot the value obtained by conventional segmentation. The study of the interaction between filtering and image sharpening (which is a current research subject for the method) will also be of interest.

Acknowledgments

We gratefully acknowledge the Italian Ministry of Education, University and Research for the support provided throughout the Project "Department of Excellence LIS4.0 - Lightweight and Smart Structures for Industry 4.0" (CUP: D56C18000400006).

References

[1] Arias-Castro, E., Donoho, D.L., 2009. Does median filtering truly preserve edges better than linear filtering? Annals of Statistics 37, 1172–1206. doi:10.1214/08-AOS604.

[2] Bacciaglia, A., Ceruti, A., Liverani, A., 2019. A systematic review of voxelization method in additive manufacturing. Mechanics and Industry 20, 630. doi:10.1051/meca/2019058.

[3] Bourell, D., Kruth, J.P., Leu, M., Levy, G., Rosen, D., Beese, A.M., Clare, A., 2017. Materials for additive manufacturing. CIRP Annals - Manufacturing Technology 66, 659–681. doi:10.1016/j.cirp.2017.05.009.

[4] Buades, A., Coll, B., Morel, J.M., 2005. A review of image denoising algorithms, with a new one. Multiscale Modeling and Simulation 4, 490–530. doi:10.1137/040616024.

[5] Carmignato, S., Dewulf, W., Leach, R., 2017. Industrial X-ray computed tomography. 1 ed., Springer International Publishing, Cham, Switzerland. doi:10.1007/978-3-319-59573-3.

[6] Cover, T.M., Thomas, J.A., 2005. Entropy, Relative Entropy, and Mutual Information, in: Elements of Information Theory. 2 ed.. Wiley. chapter 2, pp. 13–55. doi:10.1002/047174882X.ch2.

[7] De Chiffre, L., Carmignato, S., Kruth, J.P., Schmitt, R., Weckenmann, A., 2014. Industrial applications of computed tomography. CIRP Annals - Manufacturing Technology 63, 655–677. doi:10.1016/j.cirp.2014.05.011.

[8] Deng, G., Cahill, L.W., 1993. An adaptive Gaussian filter for noise reduction and edge detection, in: IEEE Nuclear Science Symposium & Medical Imaging Conference, pp. 1615–1619. doi:10.1109/nssmic.1993.373563.

[9] Diwakar, M., Kumar, M., 2018. A review on CT image noise and its denoising. Biomedical Signal Processing and Control 42, 73–88. doi:10.1016/j.bspc.2018.01.010.

[10] Elliott, D.F., Rao, K.R., 1982. Fast Transforms Algorithms, Analysis, Applications. 1 ed., Academic Press.

[11] Heinzl, C., Amirkhanov, A., Kastner, J., 2018. Processing, analysis and visualization of CT data, in: Carmignato, S., Dewulf, W., Leach, R. (Eds.), Industrial X-Ray Computed Tomography. 1 ed.. Springer, Cham. chapter 4, pp. 99–142. doi:10.1007/978-3-319-59573-3_4.

[12] International Organization for Standardization, 2017. ISO 14253-1: Geometrical product specifications (GPS) - Inspection by measurement of workpieces and measuring equipment - Part 1: Decision rules for proving conformance or nonconformance with specifications.

[13] Joint Committee for Guides in Metrology, 2012. ISO/IEC GUIDE 98-4: Uncertainty of measurement - Part 4: Role of measurement uncertainty in conformity assessment.

[14] Kruth, J.P., Bartscher, M., Carmignato, S., Schmitt, R., De Chiffre, L., Weckenmann, A., 2011. Computed tomography for dimensional metrology. CIRP Annals - Manufacturing Technology 60, 821–842. doi:10.1016/j.cirp.2011.05.006.

[15] Leach, R.K., Bourell, D., Carmignato, S., Donmez, A., Senin, N., Dewulf, W., 2019. Geometrical metrology for metal additive manufacturing. CIRP Annals 68, 677–700. doi:10.1016/j.cirp.2019.05.004.

[16] McDonnell, M.J., 1981. Box-filtering techniques. Computer Graphics and Image Processing 17, 65–70. doi:10.1016/S0146-664X(81)80009-3.

[17] Moroni, G., Petrò, S., 2018. Segmentation-free geometrical verification of additively manufactured components by x-ray computed tomography. CIRP Annals - Manufacturing Technology 67, 519–522. doi:10.1016/j.cirp.2018.04.011.

[18] Moroni, G., Petrò, S., Polini, W., 2017. Geometrical product specification and verification in additive manufacturing. CIRP Annals - Manufacturing Technology 66, 157–160. URL: https://linkinghub.elsevier.com/retrieve/pii/S0007850617300434, doi:10.1016/j.cirp.2017.04.043.

[19] Petrò, S., Moroni, G., 2019. Volumetric tolerancing and geometric verification for additive manufacturing, in: Proceedings of the XIV AITeM Conference, Padova, Italy. pp. 1–6.

[20] Petrò, S., Moroni, G., 2020. Robustness of geometric verification by segmentation-free X-ray computed tomography. Procedia CIRP 92, 163–168. doi:10.1016/j.procir.2020.05.184.

[21] Petrò, S., Pagani, L., Moroni, G., Scott, P.J., 2021. Conformance and nonconformance in segmentation-free X-ray computed tomography geometric inspection. Precision Engineering 72, 25–40. doi:10.1016/j.precisioneng.2021.03.019.

[22] Plocher, J., Panesar, A., 2019. Review on design and structural optimisation in additive manufacturing: Towards next-generation lightweight structures. Materials and Design 183, 108164. doi:10.1016/j.matdes.2019.108164.

[23] Pluim, J., Maintz, J., Viergever, M., 2003. Mutual-information-based registration of medical images: a survey. IEEE Transactions on Medical Imaging 22, 986–1004. doi:10.1109/TMI.2003.815867.

[24] Rivas Santos, V.M., Thompson, A., Sims-Waterhouse, D., Maskery, I., Woolliams, P., Leach, R., 2020. Design and characterisation of an additive manufacturing benchmarking artefact following a design-for-metrology approach. Additive Manufacturing 32. doi:10.1016/j.addma.2019.100964.

[25] Schmidt, M., Merklein, M., Bourell, D., Dimitrov, D., Hausotte, T., Wegener, K., Overmeyer, L., Vollertsen, F., Levy, G.N., 2017. Laser based additive manufacturing in industry and academia. CIRP Annals - Manufacturing Technology 66, 561–583. doi:10.1016/j.cirp.2017.05.011.

[26] Takahashi, T., Masumori, A., Fujii, M., Tanaka, H., 2018. FAV (Fabricatable Voxel) File Format Specification. URL: https://www.fujixerox.com/eng/company/technology/communication/3d/fav.html.

[27] Thanh, D.N., Prasath, V.B., Hieu, L.M., 2019. A review on CT and X-ray images denoising methods. Informatica 43, 151–159. doi:10.31449/inf.v43i2.2179.

[28] Thompson, M.K., Moroni, G., Vaneker, T., Fadel, G., Campbell, R.I., Gibson, I., Bernard, A., Schulz, J., Graf, P., Ahuja, B., Martina, F., 2016. Design for Additive Manufacturing: Trends, opportunities, considerations, and constraints. CIRP Annals - Manufacturing Technology 65, 737–760. doi:10.1016/j.cirp.2016.05.004.

[29] Vaneker, T., Bernard, A., Moroni, G., Gibson, I., Zhang, Y., 2020. Design for additive manufacturing: Framework and methodology. CIRP Annals 69, 578–599. doi:10.1016/j.cirp.2020.05.006.

[30] Volume Graphics GmbH, 2020. VGStudio MAX. URL: https://www.volumegraphics.com/en/products/vgsm.html.

[31] ZMorph, 2016. Voxelizer 3D. URL: https://zmorph3d.com/voxelizer/.